$\mathcal{PT}$-Symmetric Periodic Optical Potentials

**K.G. Makris · R. El-Ganainy · D.N. Christodoulides ·
Z.H. Musslimani**

Abstract In quantum theory, any Hamiltonian describing a physical system is mathematically represented by a self-adjoint linear operator to ensure the reality of the associated observables. In an attempt to extend quantum mechanics into the complex domain, it was realized few years ago that certain non-Hermitian parity-time ($\mathcal{PT}$) symmetric Hamiltonians can exhibit an entirely real spectrum. Much of the reported progress has been remained theoretical, and therefore hasn't led to a viable experimental proposal for which non Hermitian quantum effects could be observed in laboratory experiments. Quite recently however, it was suggested that the concept of $\mathcal{PT}$-symmetry could be physically realized within the framework of classical optics. This proposal has, in turn, stimulated extensive investigations and research studies related to $\mathcal{PT}$-symmetric Optics and paved the way for the first experimental observation of $\mathcal{PT}$-symmetry breaking in any physical system. In this paper, we present recent results regarding $\mathcal{PT}$-symmetric Optics.

Keywords $\mathcal{PT}$-symmetry · Non-Hermitian · $\mathcal{PT}$-operators · Wave propagation · Guided waves · Optical lattices · Optical solitons · Periodic potentials · Gain-loss media

K.G. Makris (✉)
Optics Laboratory, School of Engineering, Swiss Federal Institute of Technology Lausanne (EPFL),
1015, Lausanne, Switzerland
e-mail: kgmakris78@yahoo.com

R. El-Ganainy
Department of Physics, University of Toronto, 60 St. George street, Toronto, Ontario, M5S 1A7, Canada

D.N. Christodoulides
College of Optics & Photonics-CREOL, University of Central Florida, Orlando, FL, 32816, USA

Z.H. Musslimani
Department of Mathematics, Florida State University, Tallahassee, FL, 32306-4510, USA

1 Introduction

One of the most fundamental assumptions of quantum theory is that the Hermiticity of every operator is directly associated with a physical observable. This is necessary given that the spectra of such self-adjoint operators (discrete and/or continuous) are real. In the case of the Hamiltonian operator, this requirement gives rise to real energy levels and ensures conservation of the total probability (or unitary evolution). In 1998, Bender and Boettcher [7] have numerically shown that a certain class of complex non-Hermitian Hamiltonians could exhibit entirely real spectrum provided they respect parity-time ($\mathcal{PT}$) symmetry. The model quantum mechanical Hamiltonian they considered [7] is given by $H_N = -\frac{\partial^2}{\partial x^2} - (ix)^N$, where N is a real constant. Bender and Boettcher have noted the following remarkable results: When $N \geq 2$ the spectrum of H is real, positive and discrete (corresponding to infinitely many bound states). If on the other hand $1 < N < 2$, then in this regime the spectrum of H is no longer purely real and starts to involve complex conjugate pairs of eigenvalues [7]. Thus, the point $N = 2$ signifies the onset of a spontaneous $\mathcal{PT}$ symmetry breaking: A phase transition from the exact to broken $\mathcal{PT}$ symmetry phase. These remarkable findings have motivated many researchers to revisit one of the most basic axioms of quantum mechanics, i.e., the Hermiticity of a Hamiltonian, in an attempt to extend the framework of quantum theory into the complex domain (see [4–11, 13, 45, 46] for review on $\mathcal{PT}$ symmetric quantum theory).

While much theoretical success has been made in the general area of non-Hermitian quantum theory, the observation of pseudo-Hermiticity in physical settings (classical or quantum) has remained elusive. Quite recently the notion of $\mathcal{PT}$ symmetry was introduced within the framework of optics [21, 22, 32, 33, 38, 39, 41]. Parity-time optical media can be achieved through a judicious inclusion of gain/loss in guided wave geometries. One such possibility is to consider waveguide arrays [17, 18] composed of $\mathcal{PT}$ symmetric periodic structures in such a way that the $\mathcal{PT}$ symmetry of the entire system is preserved. Linear and nonlinear wave propagation in such $\mathcal{PT}$ symmetric media have been studied theoretically for the one and multi spatial dimensions. In the linear regime, various exotic phenomena have been seen such as band merging, $\mathcal{PT}$ phase transition, double refraction and non-reciprocal behavior [32, 33]. In the nonlinear case, various numerical and analytical solutions have been identified [38, 39].

Most importantly, spontaneous $\mathcal{PT}$ symmetry-breaking has been experimentally observed for the first time (in any physical system) within the realm of wave optics [22, 41]. In particular, both passive [22] and active [41] optical coupled systems have experimentally demonstrated the unique properties of such non Hermitian systems such as power oscillations, phase transition and non orthogonal supermodes (see [28] for views on the experimental results reported in [41]). These findings, in turn, have stimulated considerable research activity in the general area of $\mathcal{PT}$ optical potentials and led to several theoretical predictions such as for example: $\mathcal{PT}$ symmetry-breaking in disordered lattices [12], Bloch oscillations, transport and localization in complex crystals [29, 30], spectral singularities in non Hermitian Friedrichs-Fano-Anderson model and complex potentials [31, 36, 37], $\mathcal{PT}$ symmetric wave chaos [44], visualization of branch points in $\mathcal{PT}$ symmetric waveguides [25] and subdiffraction and spatial filtering in gain/loss media [42].

In this paper, we present recent results in the emerging field of $\mathcal{PT}$-symmetric Optics. The stationary, as well as, the dynamical of optical guided waves in $\mathcal{PT}$-lattices are investigated in detail. Band merging, double refraction, non-reciprocity, biorthogonality relations are analytically and numerically examined. The orthogonality conditions are analytically proved for a single cell, a finite and an infinite lattice, along with the projection coefficients

and the completeness relations. Some of the peculiarities of the diffraction dynamics arising in $\mathcal{PT}$-lattices such as non-reciprocity, power oscillations and phase dislocations are also discussed. Finally, nonlinear $\mathcal{PT}$-symmetric optics and solitons are presented.

2 $\mathcal{PT}$ Symmetry in Optics

In optics, the paraxial equation of diffraction is mathematically isomorphic to that of quantum Schrödinger equation. Motivated by this fact, Christodoulides group has recently suggested the possibility of realizing $\mathcal{PT}$-symmetric structures within the realm of optics [21, 32, 33, 38]. In these studies it was shown that optical $\mathcal{PT}$-synthetic materials could lead to new phenomena not possible in standard systems. Such effects include double refraction, power oscillations, eigenfunction unfolding, and non-reciprocal diffraction patterns to mention a few [32, 33]. In addition, $\mathcal{PT}$-configurations are described by a unique algebra and hence much of their behavior (including their coupled mode analysis) has to be properly derived from first principles [21]. The proposed optical $\mathcal{PT}$ systems can be realistically implemented through a judicious inclusion of gain/loss regions in guided wave geometries [32, 33]. In the suggested optical analogy the complex refractive index distribution plays the role of the optical potential. The parity-time condition implies that the real index profile should be even in the transverse direction while the loss/gain distribution must be odd. Gain/loss levels of approximately ± 40 cm^{-1} at wavelengths of ≈ 1 μm, that are typically encountered in standard quantum well semiconductor lasers or semiconductor optical amplifiers and photorefractive crystals should be sufficient to observe $\mathcal{PT}$ behavior [18, 43]. Optical nonlinearities (quadratic, cubic, photorefractive etc.) provide an additional degree of freedom since they may allow one to study such configurations under nonlinear conditions [17, 18].

Observation of $\mathcal{PT}$ symmetry breaking in complex optical potentials was first reported by Guo et al. [22] in an AlGaAs coupled waveguide system. This structure involved two weakly guided waveguide arms each designed to be single-moded at the operating wavelength of $\lambda = 1.55$ μm. One of the waveguides was always transparent while the loss in the second one was gradually increased to very high values (~ 50 cm^{-1}). To do so, chromium was deposited on one of the arms. Chromium is known for its very high imaginary part in its permittivity which also happens to be much greater than its corresponding real part. This metal was used so as to introduce appreciable losses while avoiding any unbalancing effects in the refractive index that may in turn disturb the required $\mathcal{PT}$ symmetry. Even though this arrangement involves only loss, it can nevertheless be mapped on a $\mathcal{PT}$ configuration via a straightforward transformation [22]. The total power from both channels of this system was then collected and analyzed as a function of waveguide loss. The normalized transmission results indicated a strong non-Hermitian behavior. As the loss in the dual complex potential was initially increased, a decay of the total output transmission occurred as expected. Yet, past a critical point ($\mathcal{PT}$ threshold) the transmission was found to increase. Loss enhanced transmission is in this case a direct manifestation of $\mathcal{PT}$ non-Hermiticity. At the transition point the symmetry of the structure is lost via passive $\mathcal{PT}$-symmetry breaking, and coupling between the waveguide channels begins to be reduced.

In a subsequent study by Ruter et al., a coupled $\mathcal{PT}$ waveguide system was experimentally implemented having a balanced gain/loss profile [41]. This waveguide arrangement was realized via Ti-indiffusion on an iron-doped LiNbO$_3$ crystal. Gain was provided through photorefractive two-wave mixing at levels of several cm^{-1}, enough to compete with the coupling between channels. Loss on the other hand was naturally present in the waveguides. The

two-wave mixing process was accomplished at low pump powers so as to avoid again disturbing the index balance needed for $\mathcal{PT}$ symmetry. The system's gain was then increased in time, thus allowing one to study this arrangement both below and above the $\mathcal{PT}$ phase transition point. The complex modal profiles (amplitude and phase) were also clearly observed in this study and were found to be in good agreement with theoretically anticipated results [41].

3 Wave Propagation in Linear $\mathcal{PT}$-Symmetric Periodic Media

As previously mentioned, the analogy between quantum mechanics and optics is based on the fact that they share the same mathematical formalism. More specifically, the equation governing optical beam propagation is described by a Schrödinger-like equation, namely the paraxial equation of diffraction. Here we will primarily explore the diffraction dynamics of optical beams and waves in $\mathcal{PT}$ symmetric complex potentials in the spatial domain. In normalized units, the propagation dynamics is described by:

$$i\frac{\partial \psi}{\partial z} + \frac{\partial^2 \psi}{\partial x^2} + V(x)\psi = 0, \tag{1}$$

where ψ represents the electric field amplitude, z the propagation distance, x the spatial coordinate, and $V(x)$ the complex periodic optical potential with period D. In other words it is $V(x) = V(x + D)$. A necessary (but not sufficient) for a complex potential to be $\mathcal{PT}$ symmetric is that its real part or refractive index profile is an even function of x, while the imaginary component (loss and gain profile) is odd [7, 32, 33], i.e.,

$$V(x) = \bar{V}(-x), \tag{2}$$

where $\bar{V}(x)$ denotes the complex conjugate of $V(x)$. We define the total optical power

$$P(z) = \int_{-\infty}^{+\infty} |\psi(x, z)|^2 dx, \tag{3}$$

and the so-called "quasi-power" Q [3] as

$$Q(z) = \int_{-\infty}^{+\infty} \psi(x, z)\overline{\psi}(-x, z)dx. \tag{4}$$

Note that the quasi-power is, in general, neither positive definite nor real valued. It can be shown that the quasi-power is a conserved quantity,

$$\frac{dQ(z)}{dz} = 0, \tag{5}$$

whereas the actual total optical power is not conserved and evolves according to

$$\frac{dP(z)}{dz} = -2\int_{-\infty}^{+\infty} \text{Im}[V(x)]|\psi(x, z)|^2 dx. \tag{6}$$

At this point we have to mention that $\mathcal{PT}$-symmetric optical lattices may have entirely real spectrum as well as equally distributed gain and loss, but they are not transparent. In an

interesting study by Berry [13, 14], it was pointed out that the diffraction of optical beams in $\mathcal{PT}$ periodic potentials is not unitary and the power is not conserved. The new intensity sum rules that the amplitudes of the diffracted Bragg beams follow are analytically derived and systematically examined [14]. This power oscillation effect is a direct consequence of the non-orthogonality of the eigenmodes of any $\mathcal{PT}$-symmetric non-Hermitian system. It is also discussed in [32, 33] as well as in Sect. 5.

3.1 Floquet-Bloch Theory

To understand the properties of a periodic $\mathcal{PT}$ structure we first analyze its corresponding band structure. To do so, we look for solutions of the form

$$\psi(x, z) = \phi(x) \exp(i\beta z), \tag{7}$$

where β is the eigenvalue (propagation constant) and $\phi(x)$ is the eigenmode satisfying

$$\left[\frac{d^2}{dx^2} + V(x)\right]\phi = \beta\phi. \tag{8}$$

Equation (8) is a second order differential equation with a complex periodic coefficient $V(x)$ satisfying (2) whose two linearly independent solutions are given, according to Floquet-Bloch theory [18, 26, 27], by

$$\phi_n^{(1)}(x, k) = u_n^{(1)}(x, k)e^{ikx}, \quad \phi_n^{(2)}(x, k) = u_n^{(2)}(x, k)e^{-ikx}, \tag{9}$$

where $n \in \mathbb{Z}^+$, and $k \equiv k(\beta)$ is the so-called Bloch momentum and $u_n^{(1,2)}(x, k)$ are complex, periodic and bounded functions of x that satisfy

$$\left[\left(\frac{d}{dx} \pm ik\right)^2 + V(x)\right]u_n^{(1,2)}(x, k) = \beta_n(k)u_n^{(1,2)}(x, k), \tag{10}$$

$$u_n^{(1,2)}(x + D, k) = u_n^{(1,2)}(x, k), \quad k \in \left[-\frac{\pi}{D}, \frac{\pi}{D}\right). \tag{11}$$

It suffices to consider only one set of solutions to (8) which we write in the form

$$\phi_n(x, k) = u_n(x, k)e^{ikx}, \quad u_n(x + D, k) = u_n(x, k), \tag{12}$$

with $u_n(x, k)$ satisfying

$$\frac{d^2u_n(x, k)}{dx^2} + 2ik\frac{du_n(x, k)}{dx} + [V(x) - k^2]u_n(x, k) = \beta_n(k)u_n(x, k). \tag{13}$$

If we take the complex conjugate of (13), make the change of variables: $x \to -x, k \to -k$ and use condition (2) we find

$$\frac{d^2\bar{u}_n(-x, -k)}{dx^2} - 2ik\frac{d\bar{u}_n(-x, -k)}{dx} + [V(x) - k^2]\bar{u}_n(-x, -k) = \bar{\beta}_n(-k)\bar{u}_n(-x, -k). \tag{14}$$

In what follows, we shall distinguish between two important cases.

Real Potentials   Here $\text{Im}[V(x)] = 0$, and the spectrum of $d^2/dx^2 + V(x)$ is real and consists of the union of closed intervals called spectral bands separated by infinitely many spectral gaps [19, 20, 34]. The corresponding eigenfunctions are given by (12). The behavior of the eigenmodes ϕ_n critically depends on the choice of the wave number k. When $k(\beta)$ is real then $\phi_n(x, k(\beta))$ is a bounded function of x and the eigenvalue β is said to belong to a spectral band. On the other hand, if $k(\beta)$ is imaginary, then β is said to belongs to a spectral gap. In optics, the spectrum $\beta(k)$ is referred to as photonic band gap and is determined by numerically solving (13) subject to periodic boundary condition on the primitive cell of the lattice. Due to time-reversibility, the band gap structure is symmetric around $k = 0$, i.e., $\beta_n(k) = \beta_n(-k)$.

In general, one-dimensional periodic potentials have infinitely many gaps (in optics it is referred to as complete band gap). Finally, the Floquet-Bloch functions $\phi_n(x, k)$ satisfy the orthogonality relation:

$$\int_{-\infty}^{+\infty} \overline{\phi}_m(x, k')\phi_n(x, k)dx = \delta_{nm}\delta(k - k'). \tag{15}$$

Complex Potentials   In this case $(\text{Im}[V(x)] \neq 0)$ the Floquet-Bloch theorem is valid and the corresponding eigenfunctions of the eigenvalue problem (8) are given by (12) with complex valued $u_n(x, k)$ satisfying (13). However, since the spectral problem (8) is not self-adjoint, the band structure is not generally real. On the other hand, the $\mathcal{PT}$ symmetry condition (2) provides useful clues on the reality of the spectrum [2, 15, 16, 23, 24]. In particular, it implies that if $[\beta_n(k), \phi_n(x, k)]$ is a spectral pair of the eigenvalue (8) with complex $\beta_n(k)$ so is $[\bar{\lambda}_n(k), \bar{\phi}_n(-x, -k)]$. Therefore, as we shall analytically show later, the Floquet-Bloch modes no longer satisfy the orthogonality condition (15), but a different relation of the following type:

$$\int_{-\infty}^{+\infty} \overline{\phi}_m(-x, -k')\phi_n(x, k)dx \propto \delta_{nm}\delta(k - k'). \tag{16}$$

3.2 Band-Gap Structure

For illustration purposes we assume the periodic $\mathcal{PT}$ potential of the form

$$V(x) = 4[\cos^2 x + i V_0 \sin(2x)], \tag{17}$$

with period $D = \pi$ for both real and imaginary component and V_0 is a real constant that, without loss of generality, could be chosen to be non negative. The real (solid line) and the imaginary part (dotted line) of the $V(x)$ potential for $V_0 = 0.3$ are depicted in Fig. 1(a). We emphasize once more, that the condition $V(x) = \bar{V}(-x)$ satisfied by this potential is a necessary but not a sufficient condition for the reality of the spectrum. By using spectral methods we numerically determine the existence of a $\mathcal{PT}$ threshold (V_0^{th}), below which all the propagation eigenvalues for every band and every Bloch wave number k are real. Above this $\mathcal{PT}$ threshold, an abrupt phase transition [4–7] occurs and as a result the spectrum is partially complex in spite of the fact that $V(x) = \bar{V}(-x)$ is still valid. For the specific potential given in (17), we find a threshold of $V_0^{th} = 0.5$. In other words, for $V_0 < 0.5$, the band-structure is entirely real while for $V_0 > 0.5$ it becomes partially complex. Figure 1(b) illustrates the first two bands of this potential for two cases, i.e. when $V_0 = 0.3$ (solid-dotted line) and $V_0 = 0.5$ (solid line). Note that below V_0^{th} all the forbidden gaps are open whereas at the threshold $V_0^{th} = 0.5$ the first band gap at the edges of the Brillouin zone $k = \pm 1$ closes,
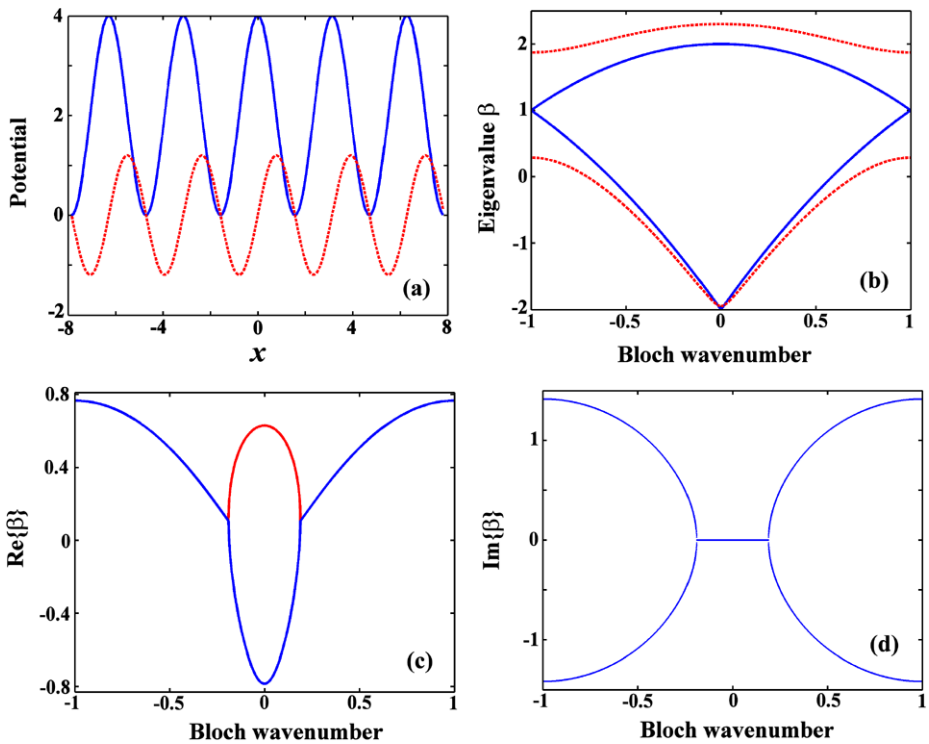
Fig. 1 (Color online) (**a**) Real (*solid line*) and imaginary (*dotted line*) component of a $\mathcal{PT}$ symmetric lattice with $V_0 = 0.3$. (**b**) The real part of the first two bands of the same potential for different values of gain/loss amplitude $V_0 = 0.3$ (*solid-dotted lines*) and $V_0 = 0.5$ (*solid lines*). (**c**) Real part of the first two bands for $V_0 = 0.85$, and (**d**) the corresponding imaginary parts of the bands presented in (**c**)

as shown in Fig. 1(b). Moreover, when V_0 exceeds this critical value the first two bands start to merge together forming an oval-like double-valued band with an associated complex spectrum. The real as well as the imaginary parts of such a band are depicted in Figs. 1(c) and 1(d), respectively when $V_0 = 0.85$. These figures show that the propagation eigenvalues are entirely real in the double valued regions, while along the overlapped sections they come in complex conjugate pairs. Note that the spectrum becomes complex after passing the $\mathcal{PT}$ threshold, starting from the lowest bands. More specifically, the first two bands form a double-valued band after the threshold while the rest of the bands have real eigenvalues. For higher values of V_0, a secondary threshold exists above of which the third and fourth bands merge together forming another double-valued structure. This process repeats as the value of V_0 further increases.

The peculiar characteristics of the corresponding Floquet-Bloch (FB) modes are also of importance. Figure 2 shows the FB modes of the first band, for Bloch wave numbers $k = -1, \pm 0.5, 0$. We also plot the structure of these modes below $V_0 = 0.49$ (Fig. 2(a)–(c)) and above $V_0 = 0.85$ (Fig. 2(d)–(f)) the $\mathcal{PT}$ threshold. Unlike real potentials, the eigenfunctions have no zero nodes at $k = \pm \pi / D = \pm 1$ (edge of the Brillouin zone), as we can clearly see in Fig. 2(a). Above the phase transition point, the FB modes with the same eigenvalue $\beta_n(k)$ form complex conjugate pairs, the same way the first two bands do. One of these modes at $k = -1$ of the first band is shown in Fig. 2(d), where the spatial shift towards the
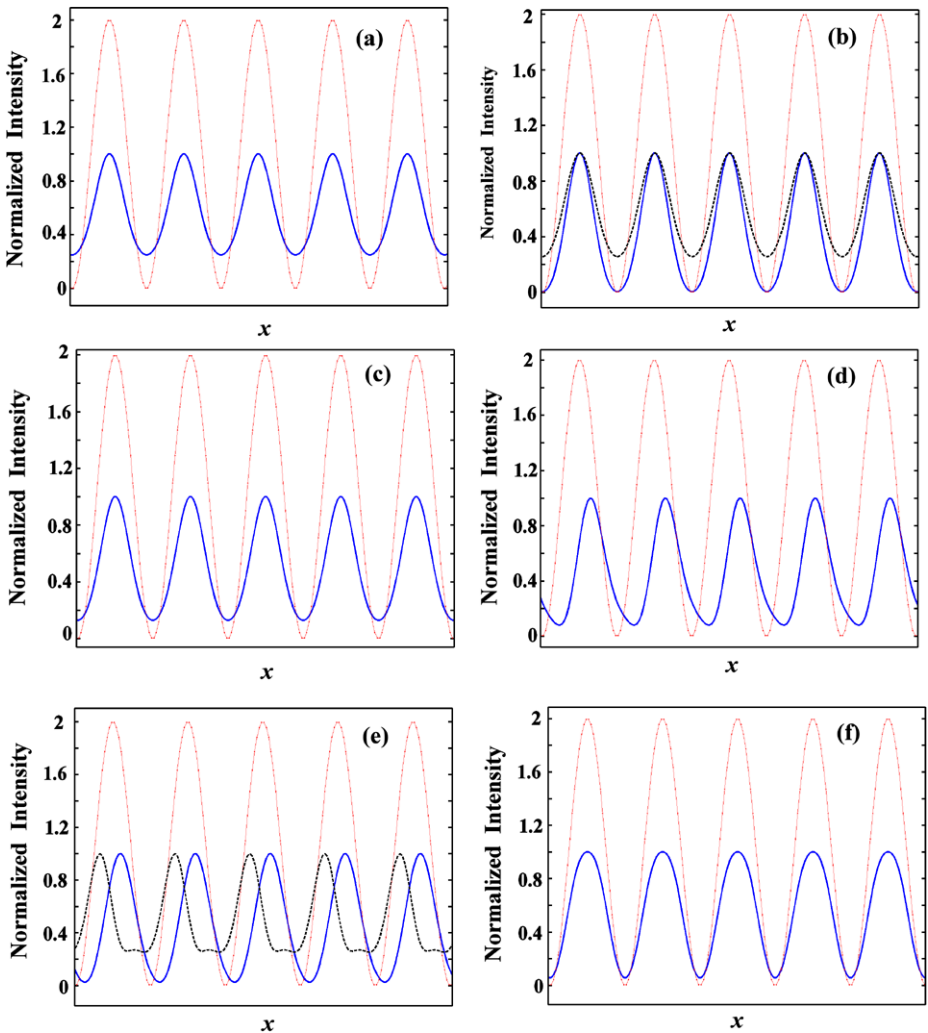
Fig. 2 (Color online) Normalized intensity profiles of FB modes of the first band of a $\mathcal{PT}$ symmetric lattice for different values of V_0, and Bloch wave numbers k. Below the $\mathcal{PT}$ threshold for $V_0 = 0.49$, FB modes with the following Bloch momentum are presented (**a**) $k = -1$, (**b**) $k = 0.5$ (*dashed line*), $k = -0.5$ (*solid line*), (**c**) $k = 0$. Above the phase transition point for $V_0 = 0.85$, we have (**d**) $k = -1$, (**e**) $k = 0.5$ (FB mode of the second band) (*dashed line*), $k = -0.5$ (*solid line*), (**f**) $k = 0$. In all cases, the real part of the periodic potential (*solid-dotted*) line is schematically depicted

loss region is apparent. The complex conjugate pair of this FB mode belongs to the second transmission band and is spatially shifted towards the gain region. An example of such a FB mode of the second band is depicted in Fig. 2(e) for the case of $k = 0.5$. We point out that, unlike in real lattices, a FB mode with Bloch wave number k is not equal to the complex conjugate of the FB mode at $-k$, i.e., $\phi_n(x, k) \neq \bar{\phi}_n(x, -k)$. For this reason we say that a band structure in a parity-time symmetric potential is non-reciprocal, with respect to the Bloch momentum k. Bloch modes corresponding to $\pm k$ wave numbers have completely different field profiles, as Figs. 2(b) and 2(e) demonstrate. We emphasize that these pecu-

liar features are a direct consequence of the non-orthogonality of the $\mathcal{PT}$ Floquet-Bloch functions. In fact, the usual orthogonality condition (15) (that is valid in real crystals) is no longer observed in $\mathcal{PT}$ symmetric lattices. This skewness of the FB modes is an inherent characteristic of $\mathcal{PT}$ symmetric periodic potentials and has important consequences on their algebra. Thus a more convenient reciprocal basis has to be developed for the inner product. This new inner product should be capable of projecting any input wavefunction on the skewed FB eigenmode basis.

A mathematical explanation for the 1/2 threshold for $\mathcal{PT}$ symmetry breaking first found in [32, 33, 38] has been recently proposed by Midya et al. [35].

4 Orthogonality of FB Modes in $\mathcal{PT}$-Periodic Potentials

In this section we discuss important issues related to orthogonality of FB modes in $\mathcal{PT}$ symmetric periodic potentials [33].

4.1 Inner Products

Let us start by rewriting (8) in the form

$$\partial_x^2 \phi_n(x, k) + V(x)\phi_n(x, k) = \beta_n(k)\phi_n(x, k), \qquad (18)$$

where $\phi_n(x, k)$ is a FB mode given by (12) and $V(x)$ satisfy condition (2). In standard Hermitian optics (when $V(x)$ is real) two different FB modes, $\phi_n(x, k)$, $\phi_m(x, k')$ satisfy the orthogonality relation (15) with respect to the inner product

$$\langle f, g \rangle = \int_{-\infty}^{+\infty} \bar{f}(x)g(x)dx, \qquad (19)$$

where $f(x)$ and $g(x)$ are two complex-valued functions. The question naturally arises as to how one could define an inner product for a complex $\mathcal{PT}$-symmetric lattice. In order to answer this question we first have to obtain the conjugate pairs associated with the Lagrangian corresponding to (18)

$$L_1 = [\partial_x \phi_n(x, k)][\partial_x \bar{\phi}_n(-x, k)] - [V(x) - \beta_n(k)]\phi_n(x, k)\bar{\phi}_n(-x, k), \qquad (20)$$

where $\partial_x \phi_n(x, k) \equiv \partial \phi_n(x, k)/\partial x$. As a result the conjugate pairs of the (18) are, $\phi_n(x, k)$, $\bar{\phi}_n(-x, k)$ and the corresponding new inner product should be defined as

$$\langle\langle f(x, k), g(x, k) \rangle\rangle = \int_{-\infty}^{+\infty} \bar{f}(-x, k)g(x, k)dx. \qquad (21)$$

Since the Floquet-Bloch theorem is valid for all periodic potentials (real and complex), it follows that every FB mode $\phi_n(x, k) = u_n(x, k)\exp(ikx)$ where $u_n(x, k) = u_n(x + D, k)$ satisfy (13). The Lagrangian corresponding to (13) is given by

$$L_2 = [\partial_x u_n(x)][\partial_x \bar{u}_n(-x, -k)] - [V(x) - k^2 - \beta_n(k)]u_n(x, k)\bar{u}_n(-x, -k)$$
$$+ 2iku_n(x, k)\partial_x \bar{u}_n(-x, -k). \qquad (22)$$

Scrutinizing (22) shows that the conjugate pairs of (13) are now different. In particular they are given by $u_n(x, k)$, $\bar{u}(-x, -k)$ and the corresponding inner product is defined by,

$$\{f(x, k), g(x, k)\} = \int_{-\infty}^{+\infty} \bar{f}(-x, -k)g(x, k)dx. \tag{23}$$

It is important to note that, for the conjugate variable, not only do we have to invert the spatial coordinate x, but the Bloch wave number k must be inverted as well. Since this inner product is different than that employed in a real lattice, the orthogonality condition is also expected to take a different form and must be systematically derived. As mentioned before, this is accomplished by first considering the orthogonality in a single cell, a finite lattice, and at the end examine the case of an infinite lattice. In all these three cases we refer always to the eigenvalue problem of (13).

4.2 Orthogonality in a Single $\mathcal{PT}$-Cell

The goal of this paragraph is to derive the orthogonality condition in one individual cell of the periodic potential defined by $\Omega \equiv [-D/2, D/2]$. Let us consider two FB modes $u_n(x, k)$, $u_m(x, k)$ belonging to different bands ($n \neq m$) but having the same wave number k. We also assume that the potential $V(x)$ is used below the $\mathcal{PT}$-phase transition point, and therefore the eigenvalue spectrum is entirely real. Then from (13) after some algebra, we finally get the orthogonality condition over a single cell in a periodic potential, that is:

$$\int_\Omega \bar{u}_m(-x, -k)u_n(x, k)dx = 0, \quad n \neq m. \tag{24}$$

Next we define the normalized FB modes as

$$\Phi_n(x, k) \equiv \frac{\phi_n(x, k)}{\sqrt{c_{kn}}}, \quad U_{kn}(x) \equiv \frac{u_n(x, k)}{\sqrt{c_{kn}}}, \quad c_{kn} \equiv \int_\Omega \bar{\phi}_n(-x, -k)\phi_n(x, k)dx. \tag{25}$$

It is easy to see that every FB function has a unique normalization coefficient c_{kn} depending on the band index n and the Bloch wave number k. In general c_{kn} are complex numbers and satisfy the symmetry relation $c_{kn} = \bar{c}_{-kn}$. Based on this normalization, (24) leads to the final orthonormality condition:

$$\int_\Omega \bar{\Phi}_m(-x, -k)\Phi_n(x, k)dx = d_{kn}\delta_{n,m}, \tag{26}$$

where

$$d_{kn} \equiv \begin{cases} 1, & \text{when } c_{kn} \in C \text{ or } c_{kn} > 0 \\ -1, & \text{when } c_{kn} < 0 \end{cases}$$

and $\delta_{n,m}$ is the Kronecker delta. As stated before, it has been numerically verified that for all FB-modes below the $\mathcal{PT}$ phase-transition point $c_{kn} \neq 0$. In other words no self-orthogonal FB modes exist in our problem [20] and the above normalization is indeed well defined.

4.3 Orthogonality in Infinite $\mathcal{PT}$-Lattices

Here we derive the orthonormality condition of two FB-modes in a $\mathcal{PT}$-symmetric infinite optical lattice. In order to do this, we calculate the corresponding inner product in a finite

lattice of N cells and then take the limit $N \to \infty$. For this purpose we consider a finite lattice with an odd number of waveguides $N = 2N' + 1$ where N' is the number of cells to the left and to the right of the central element. The width of the array is given by $L = ND$ where D is the lattice constant. First, we reduce the calculation of the inner product to an integral over just one (the central) cell, as opposed to over the entire lattice. In particular, we split the integral in every individual cell in the following fashion:

$$\int_{\substack{finite \\ lattice}} \bar{\Phi}_m(-x, -k')\Phi_n(x, k)dx$$

$$= \int_{\substack{finite \\ lattice}} \bar{U}_m(-x, -k')U_n(x, k)\exp\left[i\left(k - k'\right)x\right]dx$$

$$= \underbrace{\int_{-N'D-D/2}^{-(N'-1)D-D/2}}_{-N'\,cell} + \cdots + \underbrace{\int_{-3D/2}^{-D/2}}_{-1\,cell} + \underbrace{\int_{-D/2}^{D/2} U^*_{-k'm}(-x)\, U_{kn}(x)\, e^{i\Delta kx}dx}_{0\,(central)\,cell}$$

$$+ \underbrace{\int_{D/2}^{3D/2}}_{1\,cell} + \cdots + \underbrace{\int_{(N'-1)D+D/2}^{N'D+D/2}}_{N'\,cell},$$

where we used $\Delta k \equiv k - k'$ and $\Phi_n(x, k) = U_n(x, k)\exp(ikx)$. Given the fact that $u_n(x, k)$ is periodic with period D, every term in the summation can be reduced to an integral over the central cell by using the change of variables $x = x' - pD$ with $p = \pm 1, \pm 2, \ldots, \pm N'$:

$$\int_{\substack{finite \\ lattice}} \bar{\Phi}_m(-x, -k')\Phi_n(x, k)dx = \int_{-D/2}^{D/2} \bar{U}_m(-x, -k')U_n(x, k)e^{i\Delta kx}dx \cdot \left[\sum_{j=-N'}^{N'} e^{i\Delta kDj}\right]. \tag{27}$$

Notice that the sum of the above geometric series is well-known in Fourier analysis as the Dirichlet kernel

$$D_N(x) \equiv \sum_{m=-N}^{N} e^{ixm}, \quad x \in R,$$

and thus the integral in (27) can be written as:

$$\int_{\substack{finite \\ lattice}} \bar{\Phi}_m(-x, -k')\Phi_n(x, k)dx = D_{N'}(\Delta kD)\int_{-D/2}^{D/2} \bar{U}_m(-x, -k')U_n(x, k)e^{i\Delta kx}dx. \tag{28}$$

In order to derive the orthogonality condition in an infinite lattice we have to evaluate (28) in the limit $N' \to \infty$:

$$\int_{-\infty}^{+\infty} \bar{\Phi}_m(-x, -k')\Phi_n(x, k)dx = \lim_{N' \to \infty} \{D_{N'}(\Delta kD)\}\int_{-D/2}^{D/2} \bar{U}_m(-x, -k')U_n(x, k)e^{i\Delta kx}dx. \tag{29}$$

From the Poisson summation formula one can show that the Dirichlet kernel becomes a comb of equally spaced Dirac delta functions $\delta(x)$, namely:

$$\lim_{N' \to \infty} \{D_{N'}(x)\} = 2\pi \sum_{n=-\infty}^{+\infty} \delta(x - 2\pi n).$$

Therefore the inner product over the whole infinite lattice takes the form:

$$\int_{-\infty}^{+\infty} \bar{\Phi}_m(-x,-k')\Phi_n(x,k)dx = 2\pi \sum_{q=-\infty}^{+\infty} \delta(\Delta kD - 2\pi q)\int_{-D/2}^{D/2} \bar{\Phi}_m(-x,-k')\Phi_n(x,k)dx.$$
(30)

Since we restrict the values of the Bloch wave number only in the first Brillouin zone (reduced zone scheme), i.e. $-\pi/D \leq k < \pi/D$ it follows that $-2\pi < \Delta kD < 2\pi$. From the comb series of (30), we find that only the central term (for $q = 0$) remains. This means that

$$\int_{-\infty}^{+\infty} \bar{\Phi}_m(-x,-k')\Phi_n(x,k)dx = 2\pi \delta(\Delta kD)\int_{-D/2}^{D/2} \bar{\Phi}_m(-x,-k')\Phi_n(x,k)dx, \quad (31)$$

and since $\delta(ak) = \delta(k)/|a|$, we finally reduced the inner product calculation to one individual cell:

$$\int_{-\infty}^{+\infty} \bar{\Phi}_m(-x,-k')\Phi_n(x,k)dx = \frac{2\pi}{D}\left[\int_{-D/2}^{D/2} \bar{\Phi}_m(-x,-k')\Phi_n(x,k)dx\right]\delta(k-k'). \quad (32)$$

By combining this last relation with the orthonormality condition in one individual cell given by (26), we arrive at the orthonormality condition in an infinite $\mathcal{PT}$-lattice:

$$\int_{-\infty}^{+\infty} \bar{\Phi}_m(-x,-k')\Phi_n(x,k)dx = \frac{2\pi}{D}d_{kn}\delta_{n,m}\delta(k-k'). \quad (33)$$

It is worth mentioning that this orthonormality condition is very different than the usual one used for real periodic potentials. Here both the spatial coordinate x and the Bloch wavevector k must be reflected around the corresponding axis of symmetry.

4.4 Projection Coefficients in an Infinite $\mathcal{PT}$-Lattice

It is well known that any function can always be decomposed on a complete basis. This process is straightforward if the basis happens to be orthogonal. If, on the other hand, the eigenvectors are skewed as in the case of $\mathcal{PT}$ lattices, this decomposition becomes more involved. In this section we analyze this problem for infinite $\mathcal{PT}$ lattice and we derive and an expression for the projection coefficients.

Let us assume an infinite optical $\mathcal{PT}$ lattice with an arbitrary input field $H(x)$. This profile can be expressed as a linear superposition of the new orthonormal basis $\{\Phi_n(x,k)\}$ associated with the array and the projection coefficients $A_n(k)$ of this expansion can be uniquely determined. More specifically, any beam profile $H(x,z)$ can be written as a summation of the Floquet-Bloch modes of all bands and of all Bloch wave numbers belonging to the first Brillouin zone. This can be done via the eigenmode expansion

$$H(x,z) = \sum_{n=1}^{+\infty} \int_{-\pi/D}^{\pi/D} A_n(k)\Phi_n(x,k)\exp[i\beta_n(k)z]dk. \quad (34)$$

By multiplying both sides with the corresponding conjugate pair $\bar{\Phi}_m(-x,-k')$ and by applying the orthonormality condition of (33), we get:

$$\int_{-\infty}^{+\infty} \bar{\Phi}_m(-x,-k')H(x,z)dx = \frac{2\pi}{D}\sum_{n=1}^{+\infty} d_{k'n}\delta_{n,m}A_n(k')\exp[i\beta_n(k')z], \quad (35)$$

and the projection coefficients are given by the formula (obviously $d_{kn}^{-1} = d_{kn}$):

$$A_n(k) = \frac{D}{2\pi} d_{kn} \exp[-i\beta_n(k)z] \int_{-\infty}^{+\infty} \bar{\Phi}_n(-x, -k)H(x, z)dx. \tag{36}$$

The completeness of the FB mode basis is directly related to the Parseval's identity (different from that in real lattices):

$$Q = \frac{2\pi}{D} \sum_{n=1}^{+\infty} \int_{-\pi/D}^{\pi/D} d_{kn} A_n(k)\bar{A}_n(-k)dk, \tag{37}$$

where we define the quasi-power as $Q \equiv \int_{-\infty}^{+\infty} H(x, z)\bar{H}(-x, z)dx$ and the integrated power as $P \equiv \int_{-\infty}^{+\infty} H(x, z)\bar{H}(x, z)dx$. It is noteworthy to highlight that since the projection coefficients $A_n(k)$ are independent of z, it is easy to understand from (37) that the quasi-power Q is a conserved quantity in a $\mathcal{PT}$-lattice, while the usual power P is not. Moreover, it is straightforward to see from (36) that in general $A_n(k) \neq \bar{A}_n(-k)$ and the Parseval's identity in a $\mathcal{PT}$-lattice is not in any sense a trivial generalization of the one we have in a real periodic potential [40]:

$$P = \frac{2\pi}{D} \sum_{n=1}^{+\infty} \int_{-\pi/D}^{\pi/D} |A_n(k)|^2 dk. \tag{38}$$

The above results are derived for infinite $\mathcal{PT}$ optical lattices. However, from the computational point of view, one always deals with a finite domain and thus it is useful to reformulate the above analysis for finite lattices with periodic boundary conditions and derive the corresponding relations.

4.5 Orthonormality and Projection in a Finite $\mathcal{PT}$-Lattice

In this paragraph we analytically examine the FB mode properties of a finite $\mathcal{PT}$ symmetric periodic potential where periodic boundary conditions are imposed at the endpoints of the lattice. This approach provides a straightforward numerical implementation and calculation of the corresponding projection coefficients. The singularities of Dirac functions in the orthogonality conditions of (33) do not exist anymore and are replaced by a Kronecker delta. In the limit $N \to \infty$ the results approach that of the associated infinite lattice. Note that this methodology is widely used in the study of periodic crystals in solid state physics.

Let us assume a finite lattice of N number of cells, with $L = ND$. We here apply periodic boundary conditions at the end points of the lattice $\Phi_n(-L/2, k) = \Phi_n(L/2, k)$. By using the Floquet-Bloch theorem and the periodicity of every FB mode we get $\exp(ikL) = 1 \Rightarrow k_j = (2\pi j)/L$, $j = 0, \pm 1, \pm 2, \ldots$. But these discrete values of the Bloch wave number must belong to the first Brillouin zone $k \in [-\pi/D, \pi/D]$. This leads to the following results: $k = \frac{2\pi}{L}[-N' \ -N'+1 \ \cdots \ -1 \ 0 \ 1 \ \cdots \ N'-1 \ N']$, for odd number of cells $N = 2N'+1$, and $k = \frac{2\pi}{L}[-\frac{N}{2} \ -\frac{N}{2}+1 \ \cdots \ -1 \ 0 \ 1 \ \cdots \ \frac{N}{2}-2 \ \frac{N}{2}-1]$ for even number of cells. It is easy to see that in the first case where N is odd, the discrete k-spectrum is symmetric around $k = 0$ and $k \in (-\pi/D, \pi/D)$, whereas in the case of N being even the k-spectrum is asymmetric by one point at $k = -\pi/D$ and $k \in [-\pi/D, \pi/D)$. This asymmetry in the case of even number of cells is problematic regarding the orthogonality conditions, since in this case the FB mode $\Phi_n(x, -\pi/D)$ does not have a corresponding conjugate pair $\bar{\Phi}_n(-x, \pi/D)$. For this reason we choose a finite lattice of odd number of cells $N = 2N'+1$, with a symmetric k-spectrum.

The relation between the $\mathcal{PT}$-inner product of two different FB modes in a finite lattice (with no imposed periodic boundary conditions) with that in a single cell has been already presented in (28). Here we study how the discretization of Bloch momentum k (due to the imposed boundary conditions) affects this relation. In order to do that we have first to calculate the Dirichlet kernel $D_{N'}(\Delta kD)$ of the discrete Bloch wave number $k = \frac{2\pi}{L} \times [-N' - N' + 1 \cdots -1\,0\,1 \cdots N' - 1\,N']$. The Dirichlet kernel is given by the following relation:

$$
D_{N'}(\Delta kD) = \begin{cases} \frac{\sin[(N'+\frac{1}{2})\Delta kD]}{\sin(\Delta kD/2)}, & \text{when } \Delta kD \neq 0, \pm 2\pi, \pm 4\pi, \ldots \\ 2N' + 1, & \text{otherwise.} \end{cases}
$$

For the above discretization of the Bloch momentum k, it is straightforward to show that $\Delta kD = 2\pi s/N$, where the integer s takes the values $-2N' \leq s \leq 2N'$. Since $N = 2N' + 1 > 2N'$ it follows that ΔkD becomes zero only for $s = 0$ and is always true that $\Delta kD \neq 0, \pm 2\pi, \pm 4\pi, \ldots$ for any other non-zero value of the s integer. So when $\Delta kD = 0$, then $D_{N'}(0) = 2N' + 1$ from the above formula. On the other hand, when $\Delta kD \neq 0$ (with the $\sin(\Delta kD/2)$ denominator well defined), it is easy to see that $\sin[(N' + \frac{1}{2})\Delta kD] = 0$. By combining these two last results one can arrive at the conclusion $D_{N'}(\Delta kD) = N\delta_{k,k'}$. By substituting this relation into (28), and applying the orthonormality condition in a single cell given by (26), we get the orthonormality condition between two FB modes of different bands with different Bloch momenta in a finite lattice with imposed periodic boundary conditions, that is:

$$
\int_{\substack{finite \\ lattice}} \bar{\Phi}_m(-x, -k') \Phi_n(x, k)dx = N d_{kn} \delta_{n,m} \delta_{k,k'}. \tag{39}
$$

One convenient normalization for the FB modes is given by $\varphi_n(x, k) = \Phi_n(x, k)/\sqrt{N}$. As in the case of an infinite lattice, an arbitrary optical beam $f(x, z)$ can be expanded in terms of the finite number of FB modes (the number of FB modes is equal to the number of the cells of the lattice and also equal to the dimension of the discrete Bloch wave number k-matrix) as

$$
f(x, z) = \sum_{n=1}^{+\infty} \sum_{m=-N'}^{N'} A_{n,k_m} \varphi_n(x, k) \exp[i\beta_n(k_m)z], \tag{40}
$$

where A_{n,k_m} are the projection coefficients. By applying the orthonormality condition of (7), one can directly derive formulas for the projection coefficients and for the Parseval's identity. These are given by the following (8) and (9), respectively.

$$
A_{n,k_m} = d_{nk_m} \exp[-i\beta_n(k_m)z] \int_{\substack{finite \\ lattice}} \bar{\varphi}_n(-x, -k) f(x, z)dx, \tag{41}
$$

$$
\int_{\substack{finite \\ lattice}} \bar{f}(-x, z) f(x, z)dx = \sum_{n=1}^{+\infty} \sum_{m=-N'}^{N'} d_{nk_m} A_{n,k_m} \bar{A}_{n,-k_m}. \tag{42}
$$

The advantage of this approach is that all the relations involved can be numerically checked since the spectrum in the k-space is discrete and has finite number of FB-modes. This in turn allows us to express any beam profile as a linear superposition of FB modes and thus determine the energy content of this beam in every transmission band. As we will see, this information is useful in explaining the dynamical behavior and propagation characteristics

of optical beams in $\mathcal{PT}$-periodic potentials. At this point, we like to note that all the numerical results of the next two paragraphs regarding projection coefficients have been obtained by using a finite lattice.

5 Beam Dynamics and Power Oscillations in $\mathcal{PT}$ Optical Lattices

The most interesting aspects associated with $\mathcal{PT}$ symmetric lattices are revealed during dynamic beam evolution. Let us consider a wide (covers several channels) Gaussian beam at an arbitrary angle of incidence. Because of the non-orthogonality of the associated FB modes and the physical non-reciprocity of the lattice, we are expecting asymmetric diffraction patterns, such as double refraction and secondary emissions. For the specific periodic $\mathcal{PT}$ potential $V(x) = 4[\cos^2(x) + iV_0 \sin(2x)]$ that we consider in this paper, we examine the spatial evolution of a wide incident beam. In Figs. 3(a), 3(b) we can see the intensity distributions for two different angles of incidence, when $V_0 = 0.49$. The first one in Fig. 3(a) the diffraction pattern has a crescent-like form and is symmetric around $x = 0$ axis. On the other hand, in Fig. 3(b) the beam is splitting into three different components and the evolution is highly asymmetric. For a better understanding, we have calculated the beam's "energy content" for various bands. By applying (36), the stationary projection coefficients $|A_n(k)|^2$ can be numerically evaluated for the first three bands (where most of the "energy" of the beam is distributed). In Figs. 3(c), 3(d) the corresponding projection coefficient distributions for the input field of Figs. 3(a), 3(b), respectively, are illustrated. In Fig. 3(c) the "energy" distribution for the first two bands is symmetric with respect to the center of the Brillouin zone $k = 0$, and this is the reason for the symmetry of the resulted diffraction pattern of Fig. 3(a). Notice also that both bands have an equal contribution. For the input beam of Fig. 3(b), the projection coefficients for the first three bands are highly asymmetric. We can see that the most of the "energy" of the beam is distributed along the second band. The first and the third bands have similar secondary contributions. By taking this plot into account, one can easily explain the splitting of the beam in three new beams. The main left lobe is a result of the second band and the other two of the first and third band.

As we mentioned in a previous paragraph, the power P is not a conserved quantity in a $\mathcal{PT}$ symmetric optical lattice. So the purpose here is to understand the behavior of power with respect to the propagation distance z. This can be done analytically by calculating the integrated power with respect to the usual inner product defined in (19). The non-orthogonality of the involved FB modes plays a crucial role here. We can calculate the power of an arbitrary input beam, by expressing it as a linear superposition of non-orthogonal FB modes. The resulted formula for the integrated power P is:

$$P = \frac{2\pi}{D} \sum_{n=1}^{+\infty} \int_{-\pi/D}^{\pi/D} |A_n(k)|^2 \left(\int_{-D/2}^{+D/2} |\Phi_{kn}(x)|^2 \, dx \right) dk$$

$$+ \frac{2\pi}{D} \sum_{\substack{n=1 \\ n \neq m}}^{+\infty} \sum_{m=1}^{+\infty} \int_{-\pi/D}^{+\pi/D} A_n A_m^* \left(\int_{-D/2}^{+D/2} \bar{\Phi}_{km}(x) \Phi_{kn}(x) \, dx \right) \exp\left[i\Delta\beta_{nm}(k) z \right] dk,$$

$$(43)$$

where $\Delta\beta_{nm}(k) \equiv \beta_n(k) - \beta_m(k)$. The first term represents the usual power-spectral summation that appears in real lattice. Under the usual inner product and orthogonality relations
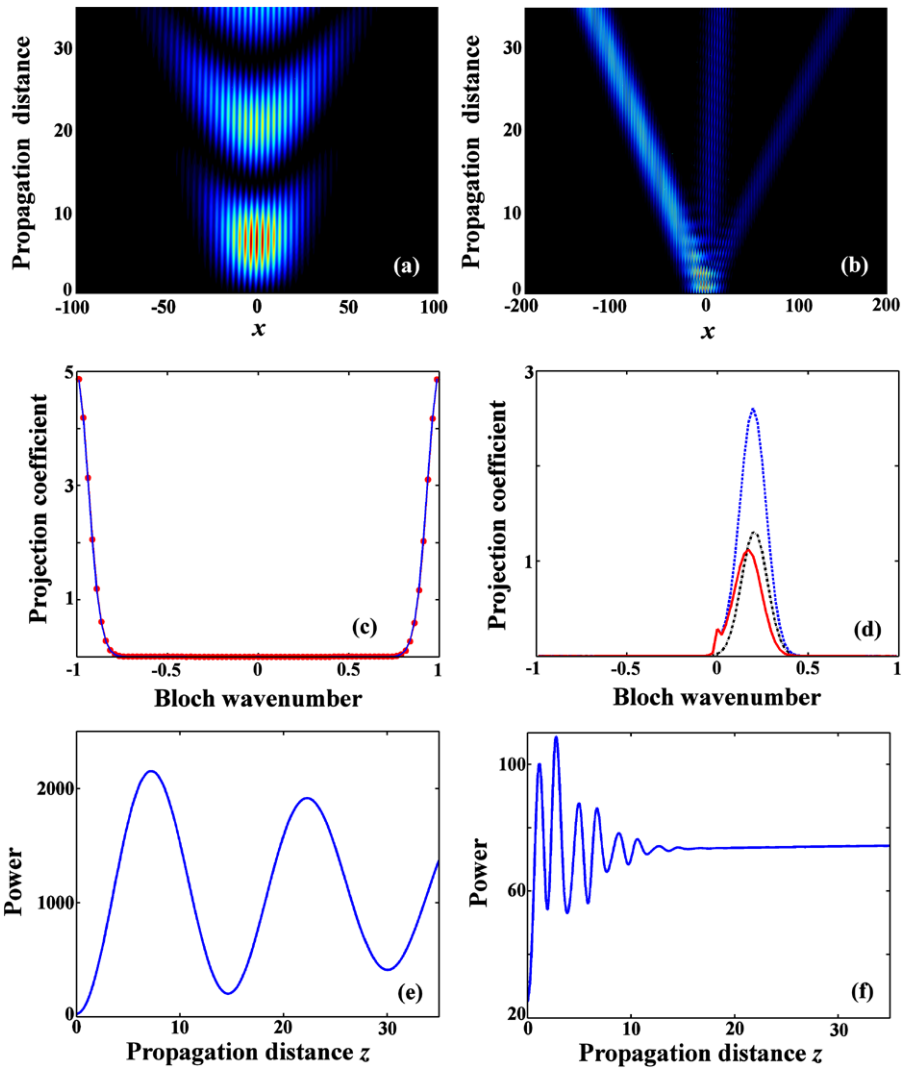
Fig. 3 (Color online) Peculiar diffraction patterns in a $\mathcal{PT}$ symmetric lattice under wide beam excitation, for $V_0 = 0.49$ (below the phase transition point). Intensity evolution of two different input beams, which lead to (**a**) crescent-like pattern, and (**b**) 3-beam splitting. The corresponding projection coefficient diagrams for these two input beams are depicted for the (**c**) first band (*solid line*), second band (*dotted line*) and (**d**) first band (*dashed-dotted line*), second band (*dotted line*), third band (*solid line*), respectively. The integrated power oscillations, with respect to the propagation distance, (**e**), (**f**) for the input beams of (**a**), (**b**), respectively

in a real lattice, the second term of (43) is zero and $\int_\Omega |\Phi_n(x,k)|^2 dx = 1$. So the above relation is reduced to the Parseval's identity in a real lattice. In a $\mathcal{PT}$ lattice, the FB modes are not orthogonal and hence some interference effects are expected. This interference between "skewed" FB modes is described by the second term of (43). Because of this term the power P oscillates in z. The oscillations are not periodic in principle. The fact that the integrated power oscillates with distance is even more surprisingly given the fact that the eigenvalue spectrum is entirely real (below $\mathcal{PT}$-phase transition point). In order to develop a better
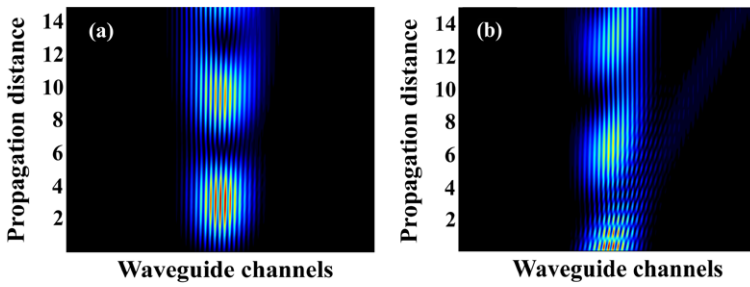
Fig. 4 Intensity evolution of wide beams exciting a $\mathcal{PT}$ lattice at angle θ when $V_0 = 0.45$ and (**a**) $\theta = 2°$, (**b**) $\theta = -2°$

understanding of this behavior, let us consider two specific examples of power oscillations in a $\mathcal{PT}$-periodic potential of the form $V(x) = 4[\cos^2(x) + i V_0 \sin(2x)]$, with $V_0 = 0.49$, that is excited by a wide optical beam. More specifically, we are interested in two different cases, the first of which is when the input beam profile leads to strong power oscillations and second is exactly the opposite. In both situations, the potential parameters are kept fixed. The intensity evolution patterns of these two beams are illustrated in Fig. 3(a) and Fig. 3(b), respectively. Notice that these patterns can be spatially symmetric or asymmetric, depending on their modal "energy" distributions among the various bands. Figure 3(e), and Fig. 3(f) depict the power oscillations of the first (Fig. 3(a)) and the second beam (Fig. 3(b)).

A direct consequence of the "skewness" of FB modes is non-reciprocity. Figure 4 shows beam propagation in a $\mathcal{PT}$ lattice when excited by a wide beam at $\pm\theta$ angle of incidence (in this case 2° degrees). Note that the two diffraction patterns are different and hence, light propagating in $\mathcal{PT}$ symmetric arrays can distinguish left from right. This is another general property of such pseudo-Hermitian optical systems.

Another interesting feature of wave propagation in $\mathcal{PT}$ symmetric periodic potentials is the existence of phase dislocations in the evolution pattern. More specifically, we examine the diffraction of a wide tilted Gaussian beam propagating in the same lattice define before. Figures 5(a), 5(b) show the intensity and the phase of the diffracted field, respectively. When the beam splits in two different parts (Fig. 5(a)), then the field at this point is zero. Consequently, the phase is undetermined and singularities appear. In the specific case, we have two phase dislocations with the same "topological charge" [Fig. 5(b)]. On the other hand, when the tilt of the beam slightly changes we get similar diffraction pattern (Fig. 5(c)), but the "topological charge" of the phase singularities has opposite sign than that in Fig. 5(b) [Fig. 5(d)]. It is noteworthy here that such characteristics and diffraction patterns have no analogue whatsoever in real Hermitian optical lattices.

6 Wave Propagation in Nonlinear $\mathcal{PT}$-Symmetric Periodic Media

In this section we study optical wave propagation in a self-focusing Kerr nonlinear $\mathcal{PT}$ symmetric potential, in which case, the beam evolution is governed by the following normalized nonlinear Schrödinger-like equation,

$$i\frac{\partial \psi}{\partial z} + \frac{\partial^2 \psi}{\partial x^2} + V(x)\psi + g|\psi|^2\psi = 0, \tag{44}$$
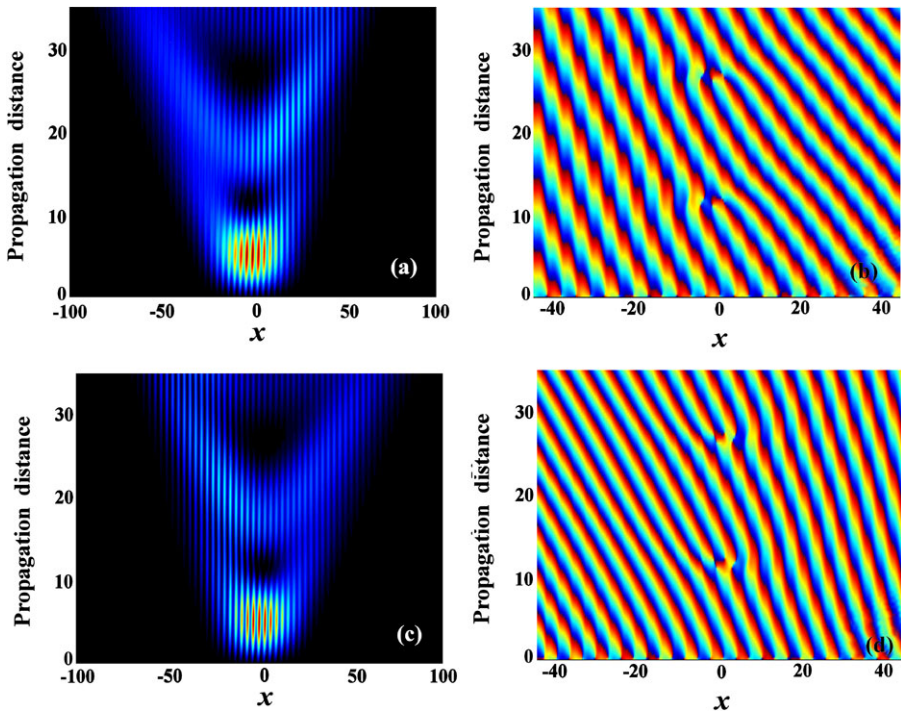
Fig. 5 (Color online) Diffraction patterns under wide beam excitation of a $\mathcal{PT}$ symmetric lattice for $V_0 = 0.49$. The evolution of (**a**) the intensity and (**b**) the phase of the diffracted field, with respect to the propagation distance are shown. Notice the two phase singularities at the points where the field is zero. The phase at these points is undetermined. (**c**) Intensity pattern of a different input beam, and (**d**) phase of the corresponding propagating field (**c**). The phase singularities here have "topological charge" of opposite sign than these illustrated on (**b**)

where ψ is proportional to the electric field envelope, z is a scaled propagation distance and $g = +1$ corresponds to a self-focusing nonlinearity while $g = -1$ to a defocusing one. We assume that the potential $V(x)$ is a complex valued function of the real variable $-\infty < x < +\infty$, $\mathcal{PT}$ symmetric and satisfy condition (2). Note that the quasi power $Q(z)$ defined by (4) evolve according to:

$$i\frac{dQ}{dz} = -g \int_{-\infty}^{+\infty} \psi(x,z)\bar{\psi}(-x,z)[|\psi(x,z)|^2 - |\psi(-x,z)|^2]dx, \tag{45}$$

whereas the total optical power $P(z)$ follows that of (6). Stationary soliton solutions to (44) are sought in the form

$$\psi(x,z) = \Psi(x,\lambda)e^{i\lambda z}, \tag{46}$$

where $\Psi(x,\lambda)$ is the nonlinear eigenmode (which in general is a complex valued function) and λ is the corresponding real propagation constant (nonlinear eigenvalue). Then $\Psi(x,\lambda)$ satisfies the nonlinear eigenvalue problem

$$\left[\frac{d^2}{dx^2} + V(x) + g|\Psi(x,\lambda)|^2\right]\Psi(x,\lambda) = \lambda\Psi(x,\lambda). \tag{47}$$

Equation (47) is supplemented with the following boundary conditions: $\Psi(x, \lambda) \to 0$ as $|x| \to \infty$.

6.1 Nonlinear Localized Modes in a Single $\mathcal{PT}$ Complex Potential

Before we consider light self-trapping in complex lattices, it is important to first understand nonlinear optical beam dynamics in a single $\mathcal{PT}$ complex potential. For illustration purposes, we assume a Scarff II potential, e.g.:

$$V(x) = V_0 \operatorname{sech}^2(x) + i W_0 \operatorname{sech}(x) \tanh(x), \tag{48}$$

with V_0 and W_0 being the amplitudes of the real and imaginary part. Notice that the corresponding linear problem associated with the potential of (48) exhibits an entirely real spectrum provided that, $W_0 \leq V_0 + 1/4$. Thus for a fixed value of V_0, there exists a threshold for the imaginary amplitude W_0. Above this so-called $\mathcal{PT}$ threshold, a phase transition occurs and the spectrum enters the complex domain. Interestingly enough, even if the Scarff potential of (48) has crossed the phase transition point (its spectrum is complex), nonlinear states can still be found with real eigenvalues. In other words, the beam itself can alter the amplitude of the refractive index distribution through the optical nonlinearity. Thus for a given W_0, this new effective potential nonlinearly shifts the $\mathcal{PT}$ V_0 threshold and in turn allows nonlinear eigenmodes with real eigenvalues to exist. In contrast, at lower power levels the parity-time symmetry cannot be nonlinearly restored and hence remains broken. It is important to note that (47) with $\mathcal{PT}$ potential (48) admits an exact solution of the form

$$\Psi(x, \lambda = 1) = \sqrt{2 - V_0 + W_0^2/9} \operatorname{sech}(x) \exp\left[\frac{i W_0 \tan^{-1}(\sinh(x))}{3}\right]. \tag{49}$$

7 Two Dimensional $\mathcal{PT}$-Symmetric Potentials

In this section we study linear and nonlinear wave propagation in two-dimensional (2D) $\mathcal{PT}$ symmetric potentials. In particular we discuss the corresponding band structure and its dependence on the potential parameters, power flow and the formation of localized structures. We end this section by giving some two-dimensional periodic exact solutions to the $\mathcal{PT}$ invariant two-dimensional NLS equation.

7.1 Linear Properties of $\mathcal{PT}$ Waveguide Arrays

Linear wave propagation in two-dimensional $\mathcal{PT}$ symmetric potentials is governed by the 2D linear $\mathcal{PT}$ invariant Schrödinger equation that is given as a simple generalization of (1) to 2D:

$$i \frac{\partial \psi}{\partial z} + \nabla^2 \psi + V(x, y)\psi = 0, \tag{50}$$

where, as in Sect. 3, the complex valued $\psi(x, y, z)$ represents the electric field amplitude, z the propagation distance, x, y the spatial transverse coordinates, and $V(x, y)$ the complex periodic optical potential with period D in both x and y; $\nabla^2 = \partial^2/\partial x^2 + \partial^2/\partial y^2$ is the two-dimensional Laplacian and the optical periodic potential $V(x, y)$ satisfies the $\mathcal{PT}$ symmetry requirement:

$$V(x, y) = \bar{V}(-x, -y). \tag{51}$$
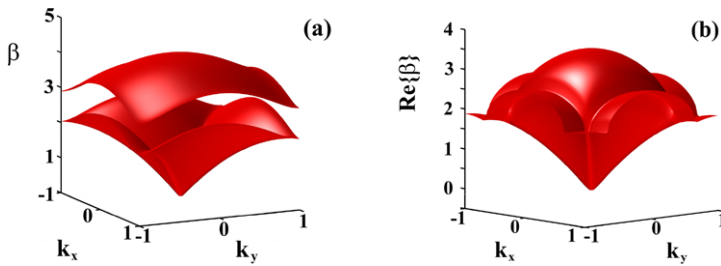
Fig. 6 Two-dimensional bandstructures associated with $V(x, y)$, for **(a)** $V_0 = 0.45$, and **(b)** $V_0 = 0.6$

To understand the properties of a two-dimensional periodic $\mathcal{PT}$ structure we first analyze its corresponding band structure. To do so, we look for solutions of the form

$$\psi(x, y, z) = \phi(x, y) \exp(i\beta z), \tag{52}$$

where β is the eigenvalue (propagation constant) and $\phi(x, y)$ is the eigenmode satisfying

$$[\nabla^2 + V(x, y)]\phi = \beta\phi. \tag{53}$$

Using the Floquet-Bloch theorem one can readily write down the solutions to (53) as

$$\phi(x, y, \vec{k}) = u(x, y, \vec{k})e^{i(k_x x + k_y y)}, \tag{54}$$

$$u(x + D, y + D, \vec{k}) = u(x, y, \vec{k}), \tag{55}$$

where $\vec{k} \equiv \vec{k}(\beta) = (k_x(\beta), k_y(\beta))$ and $u(x, y, \vec{k})$ satisfies

$$\left[(\nabla + i\vec{k})^2 + V(x, y)\right]u(x, y, \vec{k}) = \beta(\vec{k})u(x, y, \vec{k}), \quad \vec{k} \in \left[-\frac{\pi}{D}, \frac{\pi}{D}\right) \times \left[-\frac{\pi}{D}, \frac{\pi}{D}\right). \tag{56}$$

Equation (56) is supplemented with periodic boundary condition in both x and y, i.e., condition (55). In the following examples we consider the complex $\mathcal{PT}$ symmetric potential

$$V(x, y) = 4\{\cos^2(x) + \cos^2(y) + i V_0[\sin(2x) + \sin(2y)]\}. \tag{57}$$

Numerical analysis reveals that the threshold in this separable 2D case is again $V_0^{th} = 0.5$. The real part of the band structure corresponding to this potential is shown in Fig. 6 for two cases, below and above threshold ($V_0 = 0.45$ and $V_0 = 0.6$). Again below threshold the eigenvalue spectrum is real while at $V_0^{th} = 0.5$ the two bands collide at the edges of the Brillouin zone, Fig. 6(a). On the other hand, above the phase transition point (at $V_0 = 0.6$) the first two bands merge thus forming a two-dimensional oval double-valued surface (upon which all the propagation constants are real) attached to a 2D membrane where the complex conjugate eigenvalues reside (see Fig. 6(b)). The double refraction process in such 2D pseudo-Hermitian structures $V_0 = 0.45$ is shown in Fig. 7(a) when the system is excited by a normally incident wide 2D Gaussian beam. As opposed to the familiar 2D discrete diffraction pattern occurring in real lattices (Fig. 7(b) with $V_0 = 0$), in the $\mathcal{PT}$ case, two significant secondary lobes are produced only in the first quadrant. This is of course another manifestation of parity-time symmetry.
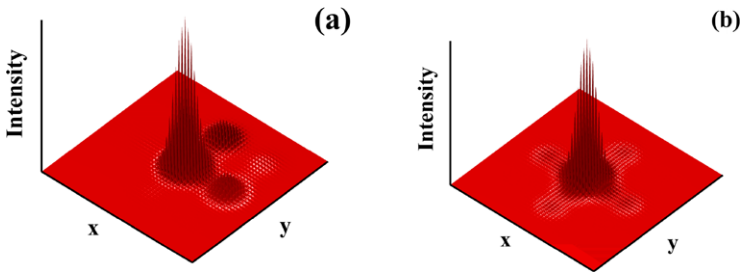
Fig. 7 Output intensity profiles: (**a**) for the 2D $\mathcal{PT}$ potential $V(x, y)$ with $V_0 = 0.45$, and (**b**) for the corresponding real lattice $V_0 = 0$

7.2 Two-Dimensional $\mathcal{PT}$ Lattice Solitons

In this section, we discuss the formation of $\mathcal{PT}$ lattice solitons in the presence of a two-dimensional periodic potential and Kerr self-focusing nonlinearity. In this case, (50) becomes,

$$i\frac{\partial \psi}{\partial z} + \nabla^2 \psi + V(x, y)\psi + |\psi|^2\psi = 0, \tag{58}$$

where again the periodic potential $V(x, y)$ obey the $\mathcal{PT}$ symmetry requirement (51). Stationary lattice soliton solutions to (58) are sought in the form $\psi(x, y, z) = \phi(x, y, \lambda) \times \exp(i\lambda z)$, where $\phi(x, y, \lambda)$ is the nonlinear eigenmode and λ is the corresponding real propagation constant. In this case $\phi(x, y, \lambda)$ satisfies the nonlinear eigenvalue problem $\nabla^2\phi + V(x, y)\phi + |\phi|^2\phi = \lambda\phi$, subject to the boundary condition: For fixed λ, $\phi(x, y, \lambda) \to 0$ as $x^2 + y^2 \to +\infty$. Before computing soliton solutions, we first solve the corresponding linear eigenvalue problem and determine the band structure. Proceeding in a similar fashion as outlined in Sect. 7.1, we have numerically determined the band structure corresponding to the periodic potentials $V(x, y) = \cos^2(x) + \cos^2(y) + iW_0[\sin(2x) + \sin(2y)]$ for the case $W_0 = 0.3$. Localized solutions to (58) can be readily constructed by extending the spectral renormalization scheme [1] to two dimensions.

A two-dimensional $\mathcal{PT}$ symmetric lattice soliton with eigenvalues within the semi-infinite gap can be numerically be found. At low intensities, the nonlinearity is not strong enough and hence this beam asymmetrically diffracts in this complex lattice. At soliton power levels however, this nonlinear wave propagates in a stable fashion.

8 Conclusions

A review of recent results regarding $\mathcal{PT}$-symmetric Optics was presented. In particular, linear and nonlinear wave propagation in $\mathcal{PT}$ symmetric optical waveguide arrays has been thoroughly studied. This was done by utilizing the formal (mathematical) analogy between the paraxial wave equation of diffraction and the Schrödinger equation. In these studies it was shown that optical synthetic materials can lead to altogether new behavior that is impossible in Hermitian optical systems. Such effects include double refraction, power oscillations, eigenfunction unfolding and non reciprocal diffraction patterns. By using the Floquet-Bloch theorem, we were able to construct the band structure of a $\mathcal{PT}$ symmetric one and two-dimensional optical potentials and identify their point of $\mathcal{PT}$ symmetry breaking. Using the spectral renormalization method, we were also able to numerically construct a family of

$\mathcal{PT}$ lattice solitons with propagation constant (or nonlinear eigenvalue) residing in the gap of the band structure.

References

1. Ablowitz, M.J., Musslimani, Z.H.: Spectral renormalization method for computing self-localized solutions to nonlinear systems. Opt. Lett. **30**, 2140–2142 (2005)
2. Ahmed, Z.: Energy band structure due to a complex, periodic, PT invariant potential. Phys. Lett. A **286**, 231–235 (2001)
3. Bagchi, B., Quesne, C., Znojil, M.: Generalized continuity equation and modified normalization in PT-symmetric quantum mechanics. Mod. Phys. Lett. A **16**, 2047 (2001)
4. Bender, C.M.: Introduction to PT symmetric quantum theory. Contemp. Phys. **46**, 277–292 (2005)
5. Bender, C.M.: Four easy pieces. J. Phys. A, Math. Gen. **39**, 9993–10012 (2006)
6. Bender, C.M.: Making sense of non Hermitian Hamiltonians. Rep. Prog. Phys. **70**, 947–1018 (2007)
7. Bender, C.M., Boettcher, S.: Real spectra in non-Hermitian Hamiltonians having PT symmetry. Phys. Rev. Lett. **80**, 5243–5246 (1998)
8. Bender, C.M., Brody, D.C., Jones, H.F.: Must a Hamiltonian be Hermitian? Am. J. Phys. **71**, 1095–1102 (2003)
9. Bender, C.M., Brody, D.C., Jones, H.F., Meister, B.K.: Faster than Hermitian quantum mechanics. Phys. Rev. Lett. **98**, 040403 (2007)
10. Bender, C.M., Hook, D.W., Meisinger, P.N., Wang, Q.H.: Complex correspondence principle. Phys. Rev. Lett. **104**, 061601 (2010)
11. Bender, C.M., Hook, D.W., Meisinger, P.N., Wang, Q.H.: Probability density in the complex plane. Ann. Phys. (2010)
12. Bendix, O., Fleischmann, R., Kottos, T., Shapiro, B.: Exponentially fragile PT symmetry in lattices with localized eigenmodes. Phys. Rev. Lett. **103**, 030402 (2009)
13. Berry, M.V.: Physics of nonHermitian degeneracies. Czech J. Phys. **54**, 1039–1047 (2004)
14. Berry, M.V.: Optical lattices with PT symmetry are not transparent. J. Phys. A, Math. Theor. **41**, 244007 (2008)
15. Boyd, J.K.: One-dimensional crystal with a complex periodic potential. J. Math. Phys. **42**, 15–29 (2001)
16. Cervero, J.M.: PT symmetry in one-dimensional quantum periodic potentials. Phys. Lett. A **317**, 26–31 (2003)
17. Christodoulides, D.N., Joseph, R.J.: Discrete self-focusing in nonlinear arrays of coupled wave-guides. Opt. Lett. **13**, 794–796 (1988)
18. Christodoulides, D.N., Lederer, F., Silberberg, Y.: Discretizing light behaviour in linear and nonlinear waveguide lattices. Nature **424**, 817–823 (2003)
19. Cottey, A.A.: Floquet's theorem and band theory in one dimension. Am. J. Phys. **39**, 1235–1244 (1971)
20. Eastham, M.: The Spectral Theory of Periodic Differential Equations. Scottish Academic Press, Edinburgh (1973)
21. El-Ganainy, R., Makris, K.G., Christodoulides, D.N., Musslimani, Z.H.: Theory of coupled optical PT symmetric structures. Opt. Lett. **32**, 2632–2634 (2007)
22. Guo, A., Salamo, G.J., Duchesne, D., Morandotti, R., Volatier-Ravat, M., Aimez, V., Siviloglou, G.A., Christodoulides, D.N.: Observation of PT symmetry breaking in complex optical potentials. Phys. Rev. Lett. **103**, 093902 (2009)
23. Khare, A., Sukhatme, U.: Analytically solvable PT-invariant periodic potentials. Phys. Lett. A **324**, 406–414 (2004)
24. Khare, A., Sukhatme, U.: Periodic potentials and PT symmetry. J. Phys. A, Math. Gen. **39**, 10133–10142 (2006)
25. Klaiman, S., Günther, U., Moiseyev, N.: Visualization of branch points in PT symmetric waveguides. Phys. Rev. Lett. **101**, 080402 (2008)
26. Kohn, W.: Analytic properties of Bloch waves and Wannier functions. Phys. Rev. **115**, 809–821 (1959)
27. Kotani, S.: Generalized Floquet theory for stationary Schrödinger operators in one dimension. Chaos Solitons Fractals **8**, 1817–1854 (1997)
28. Kottos, T.: Broken symmetry makes light work. Nat. Phys. **6**, 166–167 (2010)
29. Longhi, S.: Bloch oscillations in complex crystals with PT symmetry. Phys. Rev. Lett. **103**, 123601 (2009)
30. Longhi, S.: Dynamic localization and transport in complex crystals. Phys. Rev. B **80**, 235102 (2009)
31. Longhi, S.: Spectral singularities in a non-Hermitian Friedrichs-Fano-Anderson model. Phys. Rev. B **80**, 165125 (2009)

32. Makris, K.G., El-Ganainy, R., Christodoulides, D.N., Musslimani, Z.H.: Beam dynamics in PT symmetric optical lattices. Phys. Rev. Lett. **100**, 103904 (2008)
33. Makris, K.G., El-Ganainy, R., Christodoulides, D.N., Musslimani, Z.H.: PT symmetric optical lattices. Phys. Rev. A **81**, 063807 (2010)
34. Meiman, N.N.: The theory of one-dimensional Schrödinger operators with a periodic potential. J. Math. Phys. **18**, 834–848 (1977)
35. Midya, B., Roy, B., Roychoudhury, R.: A note on the PT invariant periodic potential $V(x) = 4\cos^2 x + 4iV_0 \sin 2x$. Phys. Lett. A **374**, 2605–2607 (2010)
36. Mostafazadeh, A.: Spectral singularities of complex scattering potentials and infinite reflection and transmission coefficients at real energies. Phys. Rev. Lett. **102**, 220402 (2009)
37. Mostafazadeh, A.: Resonance phenomenon related to spectral singularities, complex barrier potential, and resonating waveguides. Phys. Rev. A **80**, 032711 (2009)
38. Musslimani, Z.H., Makris, K.G., El-Ganainy, R., Christodoulides, D.N.: Optical solitons in PT periodic potentials. Phys. Rev. Lett. **100**, 030402 (2008)
39. Musslimani, Z.H., Makris, K.G., El-Ganainy, R., Christodoulides, D.N.: Analytical solutions to a class of nonlinear Schrödinger equations with PT like potentials. J. Phys. A, Math. Theor. **41**, 244019 (2008)
40. Odeh, F., Keller, J.B.: Partial differential equations with periodic coefficients and Bloch waves in crystals. J. Math. Phys. **5**, 1499 (1964)
41. Rüter, C.E., Makris, K.G., El-Ganainy, R., Christodoulides, D.N., Segev, M., Kip, D.: Observation of parity–time symmetry in optics. Nat. Phys. **6**, 192–195 (2010)
42. Staliunas, K., Herrero, R., Vilaseca, R.: Subdiffraction and spatial filtering due to periodic spatial modulation of the gain-loss profile. Phys. Rev. A **80**, 013821 (2009)
43. Ultanir, E.A., Stegeman, G.I., Michaelis, D., Lange, C.H., Lederer, F.: Stable dissipative solitons in semiconductor optical amplifiers. Phys. Rev. Lett. **90**, 253903 (2003)
44. West, C.T., Kottos, T., Prosen, T.: PT symmetric wave chaos. Phys. Rev. Lett. **104**, 054102 (2010)
45. Znojil, M.: PT symmetric square well. Phys. Lett. A **285**, 7–10 (2001)
46. Znojil, M.: A return to observability near exceptional points in a schematic PT symmetric model. Phys. Lett. B **647**, 225–230 (2007)